INSTITUTE OF PHYSICS PUBLISHING SUPERCONDUCTOR SCIENCE AND TECHNOLOGY

Supercond. Sci. Technol. **18** (2005) S376–S382 doi:10.1088/0953-2048/18/12/026

Coupled mechanical–electromagnetic–thermal–hydraulic effects in Nb_3Sn cable-in-conduit conductors for ITER

R Zanino[1], D Ciazynski[2], N Mitchell[3] and L Savoldi Richard[1]

[1] Dipartimento di Energetica, Politecnico, I-10129 Torino, Italy
[2] Euratom-CEA Association, CEA/DSM/DRFC, CEA/Cadarache, France
[3] ITER IT, Naka, Japan

E-mail: roberto.zanino@polito.it

Received 19 July 2005, in final form 17 October 2005
Published 7 November 2005
Online at stacks.iop.org/SUST/18/S376

Abstract

The crucial multi-physics problem of how to extrapolate from the performance of an isolated Nb_3Sn strand measured in the laboratory to the performance of a superconducting coil using multi-strand twisted cables is addressed here. We consider the particular case of the path going from the LMI strand to the international thermonuclear experimental reactor (ITER) toroidal field model coil (TFMC), through its associated Full Size Joint Sample, the TFMC-FSJS. Mechanical, electromagnetic and thermal–hydraulic conditions are simulated using the ANSYS, ENSIC and Mithrandir/M&M codes, respectively. At least in this case, the DC performance of the short sample turns out to be relatively close to (considering error bars) but not fully representative of that of the coil, showing higher (less compressive) effective thermal strain but also higher sensitivity to the electromechanical load.

(Some figures in this article are in colour only in the electronic version)

1. Introduction

One of the crucial problems in the design of large high-field superconducting magnets using Nb_3Sn superconductors is how to extrapolate from the performance of an isolated strand measured in the laboratory to the performance of the superconducting coil using multi-strand twisted cables. The uncertainty can be covered by generous margins but of course this implies a cost penalty that can be severe.

Within the frame of the International Thermonuclear Experimental Reactor (ITER) activities, it was proposed to bridge the extrapolation gap through the test of short (few metres long) but full-size well-instrumented conductor samples in dedicated facilities, e.g., SULTAN at Villigen PSI, Switzerland, aimed at the qualification of the particular conductor design.

However, the problem of how representative the conductor sample is for simulating conductor-in-coil conditions is still under discussion. It is addressed here by considering the particular case of the path going from the LMI strand (Lee *et al* 2000) to the Toroidal Field Model Coil (TFMC), tested in 2001 and 2002 at FZK Karlsruhe, Germany (Ulbricht *et al* 2005), through its associated Full Size Joint Sample, the TFMC-FSJS, tested in 1999 at SULTAN (Ciazynski *et al* 2000). Even so, one will still need some extrapolation in going from the Model Coil to the real ITER coil, including the fact that the two will not necessarily use the same conductor.

The nature of the problem at hand is intrinsically multi-physics, as the critical current carried by the cable will depend on the magnetic field, thermal field (temperature) and mechanical field (strain) distributions. A lot of work has been devoted in the past to the analysis of the DC performance of the TFMC (Savoldi *et al* 2002, Heller *et al* 2003, Zanino *et al* 2003b, Zanino and Savoldi Richard 2003, Duchateau *et al* 2004, Zanino *et al* 2004, Ulbricht *et al* 2005), although the assessment of the latter was originally beyond the scope of this experiment. Probably as the most important outcome of this previous work, the reduction in performance (albeit quantitatively dependent on the strand scaling used) of a Nb_3Sn conductor at increasing electromechanical load ($I \times B$) was reported for the first time and confirmed also in the case of the ITER Central Solenoid Model Coil (Zanino *et al*

2003a). The motivation for such a long series of works, spanning more than two years, comes both from the increasing experimental database—Phase I (TFMC standalone) followed by Phase II (TFMC + Euratom LCT coil)—and from varying ingredients and detail levels in the analysis; for example, different strand scalings—originally the so-called Summers scaling was used (Summers *et al* 1991), approximate treatment of magnetic field non-uniformity across the cable, etc. The above-mentioned conclusion on the coil performance comes from a now more-or-less standardized procedure where the voltage–temperature (VT) characteristics are simulated by a code using a couple of fitting parameters, one of which is roughly speaking the additional (with respect to the thermal and operational strain) compressive strain ($\varepsilon_{\text{extra}}$), which must be assumed to be applied to the cable in order to reproduce the measured conductor performance. At least part of this additional strain could be physically related to strand bending (Mitchell 2003) and the above-mentioned work has led to an empirical allowance in the conductor design criteria (ITER Design Description Document 2004).

Here, we use for the strand properties the Durham interpolative scaling. Additionally, two effects will be analysed that have not been directly measured but can still significantly affect the results, at least in principle: (1) the impact of the Nb_3Sn strain distribution *across the cable* on the TFMC performance, whose basic thermal hydraulic conditions are then interpreted from experimental data by the Mithrandir/M&M code (Savoldi and Zanino 2000), and (2) the impact of a non-uniform current distribution on the sample performance, using the ENSIC code (Schild *et al* 2000). Moreover, in view of the above discussion, the additional strain $\varepsilon_{\text{extra}}$ will be directly related to the local $I \times B$ force.

Finally, the comparison between strand, short sample and coil will be presented for the first time.

2. The LMI strand

The strand used in both the TFMC-FSJS and the TFMC, called the LMI strand, is an internal tin, Nb_3Sn strand fabricated by Europa Metalli, Italy.

There is a long history in the characterization of this strand in terms of critical properties (I_c) versus field, temperature and strain, where either a modified form of Summers scaling was used (Martinez *et al* 1997), or other types of scaling (Godeke *et al* 1998). However, only very recently it was realized in tests performed at Durham University, UK, that the strain sensitivity of the strand performance is significantly stronger than expected from Summers (Taylor and Hampshire 2005), a fact which changed the quantitative picture of the results of the coil performance analysis a little, as mentioned above.

No matter what scaling is used, it is based in any case on the characterization of a very limited number of strands, so that the average expected performance of the cable must inevitably make use of the data from the QA procedure. In the case of Summers this is customarily made by adjustment of the C_0 constant based on the average I_c measured at 12 T and 4.2 K under zero load (Duchateau *et al* 2001). In the case of the Durham scaling the issue may be trickier, but within the scope of the present paper the average I_c values from the QA of both TFMC-FSJS (152 A) and TFMC (153 A) are very close to that measured in the single-strand tests (151 A), so that no adjustment of the scaling constants given in Taylor and Hampshire (2005) is needed here.

3. Analysis of TFMC-FSJS DC performance

3.1. The TFMC-FSJS experiment

The TFMC-FSJS is a sample made of two identical conductor legs (left and right) joined at the bottom. The conductor is a typical dual-channel ITER cable-in-conduit conductor, with a multi-stage structure including 1080 strands of which 2/3 are superconducting (LMI strands) and 1/3 Cu, and a 2 mm thin circular SS conduit. The six last-but-one wrapped cabling stages are twisted around a central channel, delimited by a 1 mm thick perforated SS spiral, and called petals. Many tests were performed on this sample in the SULTAN facility, with magnetic field ranging from 7 to 11 T; however, most of the runs were dedicated to V–I characteristics and only a few to V–T characteristics (Ciazynski *et al* 2000).

The assessment of the TFMC-FSJS performances is made using the ENSIC code (Schild *et al* 2000), and the Durham scaling for the LMI strand. In these simulations, as in the TFMC ones reported below, the current was assumed in a first step to be equally shared among all the superconducting strands of the cable. The code computes the voltage between measuring taps, taking into account the SULTAN field profile and the self-field (the average voltage along the different petals is computed but the jacket is not included in the electrical model).

Although these voltage taps are about 400 mm apart and the SULTAN magnetic field is applied over about 420 mm, their dissymmetry with respect to the SULTAN field axis leads to an effective length of about 330 mm. There are two unknowns in the model: the strain of the Nb_3Sn filaments ε (assumed uniform and *constant during the run* as a first approximation), and the cable n-value. For each run, the values of these parameters are determined by the best fit of the experimental characteristic, with more weight given to the electric field within the range 10–100 μV m^{-1}.

The results for the average strain ε in the left leg of the sample are plotted in figure 1 as a function of $I_{\text{eff}} \times B_{\text{ave}}$. I_{eff} is the sample effective current (defined at an intermediate electric field of 30 μV m^{-1}) and B_{ave} is the magnetic field at the conductor centre. The error bars on ε are $\pm 0.01\%$ (absolute).

From figure 1 it can be seen first of all that ε depends approximately linearly on $I_{\text{eff}} \times B_{\text{ave}}$ in the range considered. It is worthwhile mentioning that this observation was not made at the time of the first analysis of the short-sample performances, but appeared only later, in connection with the test of the ITER Model Coils. From figure 1 it can also be noted that the first runs, up to ~#10, exhibit slightly decreasing performances, after which performances are more stable. Finally, the V–T runs give results roughly consistent with the V–I runs, which may justify the definition of I_{eff} introduced above for the V–I runs.

In a second step, in order to get a more accurate picture, we introduce a variation of ε directly in the model following equation (1).

$$\varepsilon(y) = \varepsilon_{\text{th}} + \varepsilon_{\text{extra}} = \varepsilon_{\text{th}} - \gamma I \times B_{\text{ave}}(y). \qquad (1)$$

While previous recipes, e.g., (Zanino *et al* 2004), adopted a uniform strain, in this paper ε is a function of the space coordinate y along the conductor length (through $\varepsilon_{\text{extra}}$) and it is also varying in time (through I) in the case of the V–I runs. The thermal strain ε_{th} is now an unknown (instead of ε), together with the cable n value, and both must be

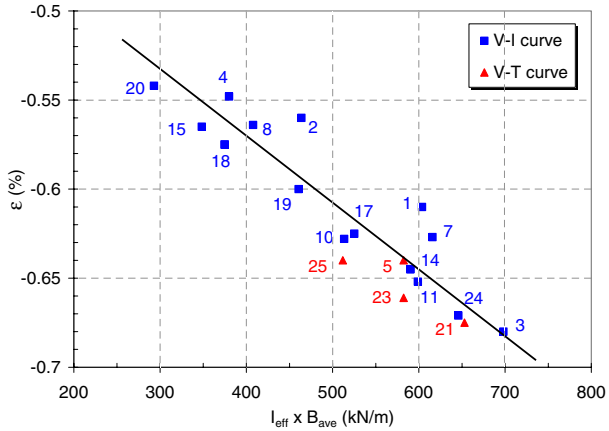

Figure 1. Best-fit ε for the TFMC-FSJS left leg (the index is the run order number). The line shows the boundary below which performances tend to stabilize.

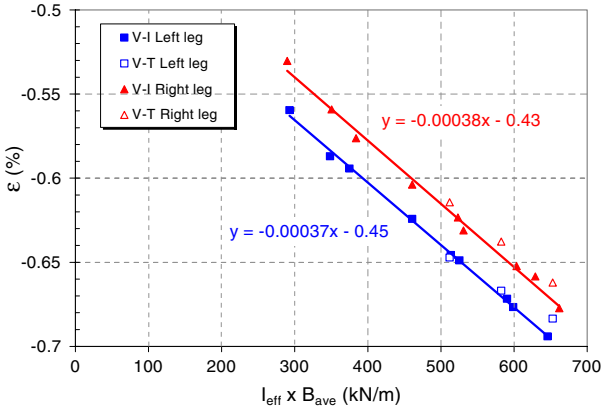

Figure 2. Result of ENSIC simulations with uniform current distribution. (The least-square fits for the right and left leg, respectively, are also reported: $x = I_{\rm eff} \times B_{\rm ave}$, $y = \varepsilon$.)

determined attempting to best fit the measured V–I and V–T characteristics.

As a first guess we take the constant $\gamma = 3.5 \times 10^{-4}$ [%(kN/m)$^{-1}$] in the left leg, and $\gamma = 3.6 \times 10^{-4}$ [%(kN/m)$^{-1}$] in the right one, based on the previous constant- (and uniform-) ε analysis. Rather similar values for $\langle\varepsilon_{\rm th}\rangle$ (the average value of $\varepsilon_{\rm th}$ among all the runs with # $\geqslant$10) are then obtained:

$$\langle\varepsilon_{\rm th}\rangle = -0.434 \pm 0.005\% \qquad \text{for the right leg}$$
$$\langle\varepsilon_{\rm th}\rangle = -0.464 \pm 0.004\% \qquad \text{for the left leg}$$

where the error bars correspond to the standard deviation of $\varepsilon_{\rm th}$. In this case, the values of n found from the V–I runs are obviously lower than in the previous analysis (the n-value ranges from 4 to 7, instead of 6 to 9), and are in agreement with those given by the V–T runs.

The final values of ε computed from (1) using the best-fit $\varepsilon_{\rm th}$ and the value of $B_{\rm ave}$ at peak SULTAN field are shown in figure 2 for the two sample legs, with run numbers $\geqslant$10. The behaviour of the two legs is similar, with slightly better performances for the right leg (the slope is essentially the same but $\varepsilon_{\rm th}$ is slightly different). The scattering can be due to extensive operating conditions (i.e. the same $I \times B_{\rm ave}$ can be obtained with different combinations of I and $B_{\rm ave}$). The values of $\varepsilon_{\rm th}$ and γ are slightly different from the analysis above since this computation can be considered as a second iteration. One can also notice that the V–T points are now better integrated to the V–I points compared to figure 1; in particular, the slight shift between V–T points and V–I points shown in figure 1 has disappeared with the more consistent model using (1). However, the slopes obtained using only the V–T points look lower than those obtained from the V–I points (quoted on the graph), but taking into account the error bars ($\pm$0.01%) and the relative closeness of the few V–T points it is hard to give a meaning to this result.

It is known from previous work on other ITER samples that a sufficient level of current non-uniformity, both among and within the petals, can affect both the $I \times B$ dependence and the $\varepsilon_{\rm th}$ offset (Mitchell 2000). The current distribution among the petals of the two conductor legs of the TFMC-FSJS can be estimated thanks to the analysis of the signals from segmented

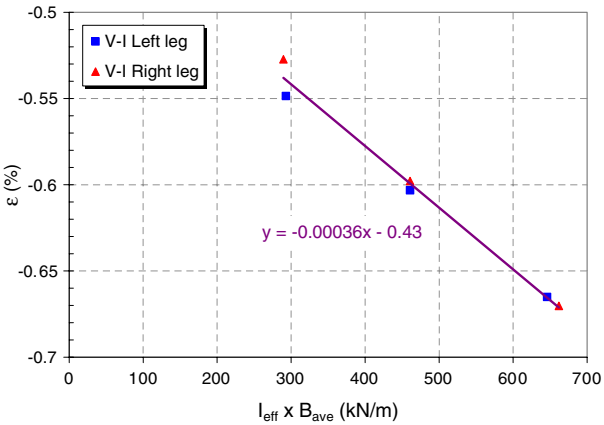

Figure 3. Best-fit ε computed with ENSIC and non-uniform current distributions. (The global least square fit is also reported: $x = I_{\rm eff} \times B_{\rm ave}$, $y = \varepsilon$.)

Rogowski coils located around the conductors (6 mini coils per leg, each corresponding to one petal). This analysis is performed by inverting the matrix giving the computed 12 coil magnetic fluxes (6 per leg) as a function of the 12 petal currents (6 per leg), assuming a uniform current distribution inside the petals. We find that the current distribution was more non-uniform in the left leg (maximum overload ~30–40%) than in the right leg (maximum overload ~10–20%). By adjusting the series resistances (in the joints) in the ENSIC model (Schild *et al* 2000), it is possible to simulate such a situation with typical current distributions $I_{\rm petal}/(I/6)$, far from $I_{\rm C}$ or from the current-sharing temperature $T_{\rm CS}$, of (1.4; 1.2; 1.0; 1.0; 0.8; 0.6) in the left leg, and (1.2; 1.1; 1.0; 1.0; 0.9; 0.8) in the right leg, respectively. Inter-petal resistances were varied within the 1–10 $\mu\Omega$ m range but without significant effects due to the short length of the sample (i.e., current redistribution is performed mainly through the joint series resistances).

A limited number of TFMC-FSJS runs was analysed with the non-uniform current model and the best-fit results of these simulations are given in figure 3. It can be seen in this figure that, within the error bars due to fitting of the V–I curves ($\varepsilon \pm 0.01\%$), and to the Rogowski analysis ($\pm$10% of petal current, roughly equivalent to $\pm$0.01% on ε), the two legs can be now considered as almost identical. This result tends to

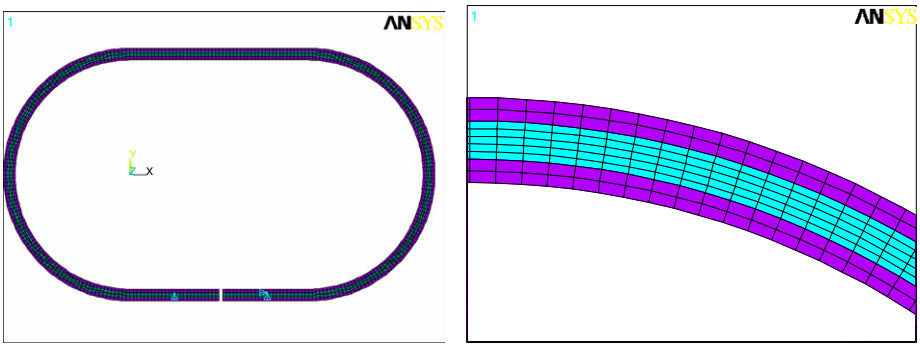

Figure 4. Finite element model showing cable and jacket.

show that the lower performance of the left leg is mainly due to a more non-uniform current distribution among its petals.

4. Analysis of TFMC DP1.2 DC performance

4.1. Mechanical model of the TFMC cable

The TFMC is a racetrack coil, which uses the same conductor as the TFMC-FSJS. In this section the mechanical behaviour of the TFMC cable inside the jacket is analysed. The first step is the use of a finite element model of the first turn of the coil. The aim of the model is to examine how the 'global' behaviour of the cable differs from that of the adjacent jacket, due to friction and gaps.

The TFMC is a difficult situation for the interpretation of cable behaviour. The high-field regions on the conductor are very localized (a length of 10 cm or so), there is a substantial field gradient across the conductor (Zanino *et al* 2004) as the current is up to 80 kA, and the peak field regions are within a curved length of conductor, where there is a significant external mechanical strain gradient (Zanino *et al* 2004) due to the bending of the coil under the magnetic loads.

A finite element model of the first (innermost) turn of the TFMC has been developed using ANSYS version 9.0 with PLANE82, LINK1, CONTACT172 and TARGET169 Elements. The model is 2D plane strain and a detail of the corresponding mesh is shown in figure 4 (y is the direction along the cable and x the orthogonal direction in the plane of the figure, i.e., orthogonal to the coil axis). The cable is enclosed in a jacket (effectively very stiff compared with the cable). The coil deformation is applied through LINK1 truss elements with an imposed initial strain taken from the global TFMC stress analysis (Raff *et al* 2001). The two parts of the jacket (inner and outer) are linked by an overlay of 2D jacket material elements. The cable–jacket surfaces (inside and out) have contact elements, which allow gaps and sliding with a defined friction coefficient. The jacket and cable are broken in the joint/transition region (so that the structure can be simply supported) and the cable is also fully bonded to the jacket in this region. The cable width is derived by assuming a square section with an area equivalent to the actual circular shape.

The global strain, computed assuming a winding pack with orthotropic material properties simulating the conductors in the radial plates with insulation material (Ulbricht *et al* 2005), is applied directly to the jacket material. The jacket has isotropic linear elastic properties with 100× the moduli of steel so that there is no extra jacket deformation from the applied transverse magnetic loads (in addition to the applied strain).

Representation of the cable by 'smeared' mechanical properties is a problem that will be readdressed below using measured data. In this first step, the cable material was assumed to be linear elastic orthotropic. Of the 21 elastic constants needed in a general 3D case only 12 values are left in the case of 2D plane strain model and they have to satisfy the constraints coming from the symmetry of the compliance matrix (e.g., $\nu_{yx}/E_y = \nu_{xy}/E_x$, etc). The local magnetic loads on the cable are calculated from the local magnetic field (Ulbricht *et al* 2005) shown in figure 5, assuming a uniform current density.

On application of the thermal loads, the cable is pressed against the curved ends of the racetrack section (giving a low pressure on the outer surface). In the straight section, there is almost full sliding as there is low contact pressure. This cable behaviour is enhanced when the magnetic loads are applied, compared to expectations based on the analysis only of the jacket behaviour. This is due to the outward movement of the cable within the jacket combined with the relatively low longitudinal stiffness of the cable compared to the supporting structures (mostly the jacket). The pressure at the curved ends reaches a maximum and the corresponding gap between the cable and the jacket on the inner surface is in reasonable agreement with previous analysis of ITER coil test results (Hamada *et al* 2002). The compression onto the outer jacket surface produces a transverse compression of the cable and allows an outward movement of the inner high-field surface. This creates a tensile strain, which offsets the thermal compression.

It is also possible to derive a simple analytical expression for this additional longitudinal strain component on the inner surface of the cable, leading to the following form of the operational strain

$$\varepsilon_{\mathrm{op}} = \text{jacket strain} + B \times I/2E_x R \qquad (2)$$

where B is the field, I is the current, E_x is the transverse elastic modulus of the cable and R is the local radius of curvature. For the TFMC this expression gives indeed an additional strain (for the reference cable), which agrees well with the finite element simulations.

However, the analysis presented so far is not completely satisfactory because of the actually non-linear behaviour of the cable transverse modulus (Nijhuis *et al* 2004), which was not included in the ANSYS model. It is indeed difficult to develop

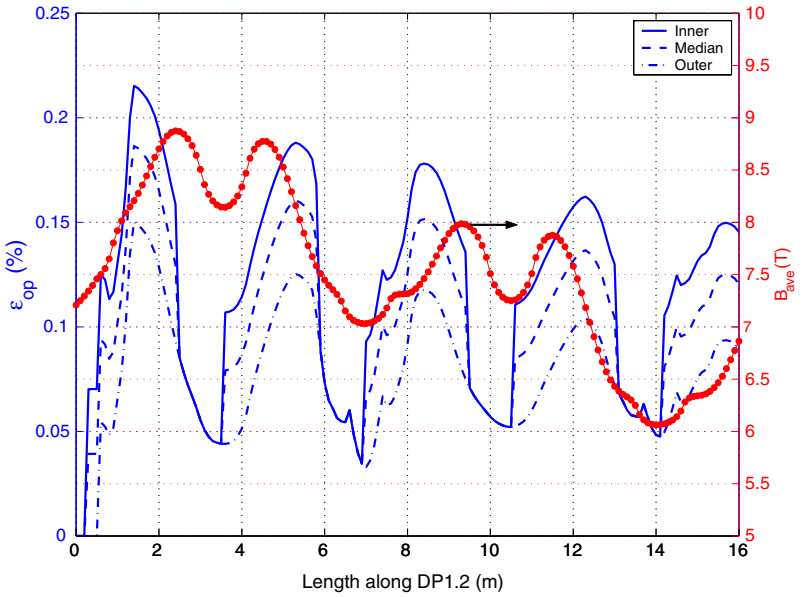

Figure 5. Distribution of the cable operating strain along the first metres of the TFMC DP1.2, computed on the inner surface (solid line), median surface (dashed line) and outer surface (dash–dotted line), respectively, for the 80/16 case. The average magnetic field along the conductor axis (symbols) is also reported.

an adequate non-linear finite element analysis of this because of the need to provide a full non-linear elasticity matrix, for which measured data are unavailable. The corrections to the longitudinal operating strain have therefore been redone using an approach based on the results of mechanical measurements of the transverse modulus of the cable, as discussed in detail in (Savoldi Richard *et al* 2005).

According to this approach, the additional operating strain in the cable is given by the following modification to equation (2):

$$\varepsilon_{op} = \text{jacket strain} + (\delta + \delta_p)/R \tag{3}$$

where δ is the elastic part of the transverse cable displacement, weakly dependent on $I \times B$ (Savoldi Richard *et al* 2005), δ_p is the permanent settlement in the cable over the first few load cycles (presumably due to plastic deformation of the strands) and R is the local radius of curvature. δ_p amounts to a maximum of 0.2–0.4 mm, depending on the sample. However, there are no data available on how it varies across the cable section and it seems appropriate to assume a variation that is proportional to δ.

Using these expressions it is possible to find the resulting operational strain distribution along and across the cable as shown in figure 5.

4.2. M&M thermal–hydraulic model and simulation strategy

The evaluation of the TFMC performance has been performed using the Multiconductor Mithrandir (M&M) code (Savoldi and Zanino 2000) for the analysis of the T_{CS} measurements, as in (Zanino *et al* 2004), (Ulbricht *et al* 2005). The model simulates simultaneously both DP1.1 and DP1.2, coupled by heat transfer through the inlet joint. For a given evolution of the inlet helium temperature, driven by the resistive heaters, it computes the full thermal–hydraulic evolution (1D compressible He flow in each channel + heat conduction in the solids) in the two pancakes and in particular the evolution of the strand temperature profile in the DP1.2 pancake.

The strain profile along the conductor for the inner, median and outer surface has been used to determine, across the conductor cross section, a parabolic fit for the strain. The coefficients of this fit vary along the conductor, in order to reproduce the global picture of figure 5.

The variable strain profile has been used in the computation of the average electrical field on each cross section, following equation (4):

$$\langle E \rangle(y) = \frac{2E_C}{\pi(R_{out}^2 - R_{in}^2)}\left[\int_{-R_{out}}^{R_{out}} (j/j_C(x,y))^n \sqrt{R_{out}^2 - x^2}\,dx - \int_{-R_{in}}^{R_{in}} (j/j_C(x,y))^n \sqrt{R_{in}^2 - x^2}\,dx\right] \tag{4}$$

where the critical current density

$$j_c(x,y) = j_c(T(y), B(x,y), \varepsilon(x,y)) \tag{5}$$

is computed according to the Durham scaling law for the LMI strand (Taylor and Hampshire 2005).

The longitudinal strain ε is the sum of three components:

$$\varepsilon(x,y) = \varepsilon_{th} + \varepsilon_{op}(x,y) + \varepsilon_{extra} \tag{6}$$

where ε_{th} is the thermal strain (here assumed to be -0.61% as in all previous assessments), ε_{op} is the operational strain as computed from equation (3) (see figure 5) and ε_{extra} is defined as a function of the local load, see equation (1). The constant γ in ε_{extra}, see equation (1), is a fitting parameter, together with the cable n-value n in equation (4), allowing the best fit of the V–T_{in} characteristic (Ulbricht *et al* 2005).

The limitations in the adoption of equation (4) consist mainly in assuming a uniform current distribution on the conductor cross section. This limitation is intrinsic to the Mithrandir/M&M model, and cannot be overcome in this analysis, but previous analysis with ENSIC showed that joint-driven non-uniformity in TFMC should be below 10% overload (Ulbricht *et al* 2005).

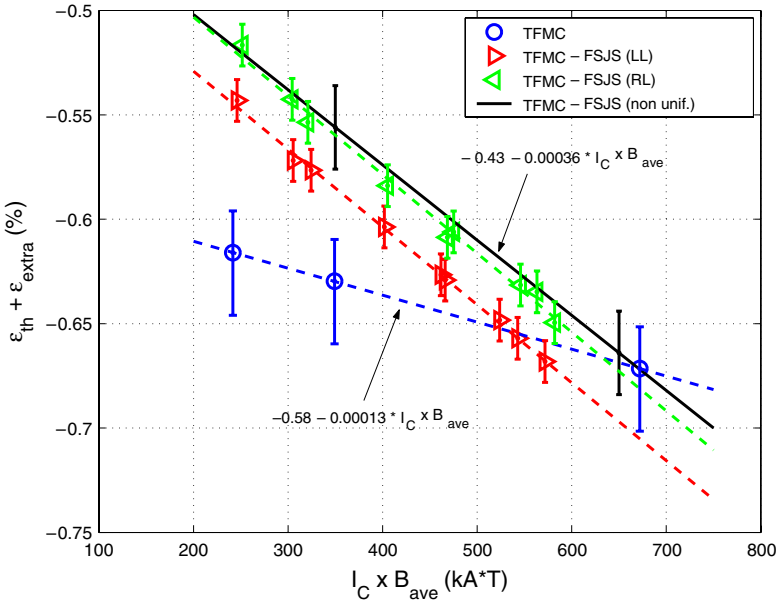

Figure 6. Comparison of TFMC short-sample and coil performance. Also the result of the non-uniform current analysis of the short sample is shown (solid line).

4.3. Analysis of the TFMC T_{CS} tests

The reassessment of the TFMC performance using the new mechanical model and local ε_{extra} has been performed in three cases: $I_{TFMC} = 80$ kA and $I_{LCT} = 16$ kA, $I_{TFMC} = 69$ kA and $I_{LCT} = 0$ kA, and $I_{TFMC} = 49$ kA and $I_{LCT} = 11$ kA.

The results in terms of $\varepsilon_{th} + \varepsilon_{extra}$ as a function of the average magnetic load ($I_{TFMC} \times B_{ave}$) at the location where T_{CS} is reached for the first time are reported in figure 6. Since ε_{th} is constant, ε_{extra} scales approximately linearly with $I \times B$, possibly due to strand bending and other factors, not included in the present mechanical model. *Assuming* a linear extrapolation (?) to the origin gives $\varepsilon_{th} \sim -0.58\%$, very close to the assumed value (-0.61%). Perhaps future short-sample tests at very low $I \times B$ could help reduce the uncertainty in this extrapolation.

Different factors affect the accuracy of the computed ε_{extra}: the accuracy on the computation of the jacket strain ($\pm 10\%$) can cause an uncertainty up to $\pm 0.01\%$; the field gradient *along the coil axis* (up to 0.1 T) can cause a reduction of -0.01% and the best-fit search itself has an error of at least $\pm 0.01\%$. The global effect on the error bars, assumed conservatively equal for all the shots, is represented in figure 6.

The M&M results in terms of n-index of the cable are reported in table 1. n is assumed constant for each run, showing comparable values to those in (Ulbricht *et al* 2005).

Table 1. Best-fit n-value for the cable from the TFMC performance reassessment.

I_{TFMC}/I_{LCT} (kA)	Cable n-value
80/16	8 ± 1
69/0	6 ± 1
49/11	5 ± 1

5. Sample versus coil comparison and discussion

The comparison between sample and coil performance is reported in figure 6 in terms of the dependence of the strain on $I_C \times B_{ave}$ (where I_C is the critical current, i.e., the current corresponding to a peak electric field level of 10 μV m^{-1}), once the operating strain ε_{op} contribution is subtracted out from the TFMC case, in order to make a coil versus sample comparison meaningful.

The sample performance appears to be better than that of the coil, which might be of some concern from the point of view of the representativity of the ITER sample performances, but the sensitivity to the electromechanical load is larger for the sample than for the coil.

The different ε_{th} in the sample ($\sim -0.45\%$) and the coil ($\sim -0.58\%$) could be due to a possible cable slip in the sample jacket and inside the joints (on the copper soles) during heat treatment. Indeed, a 1 mm slip at each end leads already to a relaxation of $\sim 0.1\%$ on ε_{th}. Countermeasures are being considered in the perspective of the future short-sample tests.

Concerning the different slope, the somewhat 'singular' behaviour appears to be that of the TFMC, while, for example, the CS Model Coil and its short sample have rather similar slope to the TFMC-FSJS, within a factor of less than 2 (Savoldi Richard *et al* 2005). Of course, several uncertainties (leading to corresponding error bars) affect both sample and coil slope. As regards the sample, for example, the influence of possible current non-uniformity *within a petal* has not been investigated (also because it is essentially impossible to diagnose experimentally). As regards the coil, the slope at given measured performance comes from the slope of ε_{op}, which in turn comes from the mechanical model. Therefore, the anomalous TFMC slope could possibly be related to a partial inadequacy of the mechanical model itself. Indeed, the short-sample performance is expected *a priori* to be substantially representative of the conductor performance in the coil, with the exception of the coil operating strains and the sample current non-uniformity. The object of the analyses presented in sections 3 and 4 is to reduce both coil and sample to

a comparable basis, leaving only the so-called transverse load ($I \times B$) degradation. There are some manufacturing variations between coil and sample, with the coil conductor undergoing mechanical disturbance after heat treatment during the transfer and insulation process, and the straight sample may allow the possibility of disengagement of jacket and cable, as discussed above. However, the operating conditions overlap.

Concerning the cable n-value, the sample and coil appear similar, but the sample has somewhat lower values. For both, the n-value turns out to be much lower than that of the strand, and increases with the critical current.

6. Conclusions and perspective

In the ITER roadmap the representativity of short-sample DC performance for real coil operation is a crucial assumption, which was investigated in this paper by comparing the TFMC-FSJS versus TFMC performance.

A non-uniform current model of the TFMC-FSJS implemented in ENSIC has been used to assess the results of I_C and T_{CS} tests of the short sample. A new mechanical model of the TFMC cable has been developed, leading to the assessment of longitudinal strain variation on the cable cross section, which is used in the M&M analysis of T_{CS} tests of the coil.

The major results of this analysis can be summarized as follows.

- ε_{th} for the sample is consistently less compressive than was assumed/estimated. We hope to reduce the uncertainty by low-$I \times B$ tests of future short samples.
- ε_{th} is less compressive in the sample than in the coil. This could be attributed to cable slip in the sample and interpretation of non-uniform current effects could be affected by voltage tap location. A much weaker $I \times B$ dependence (slope) of the strain is found for the coil compared to the sample. The sample and coil appear to agree better at high $I \times B$ (more representative of the normal operating conditions) but if the low apparent thermal strain of the sample is due to relaxation through slip, this agreement is fortuitous. The difference in the slopes probably indicates that we are still missing some modelling elements in our understanding of cable-in-conduit conductor behaviour.

The above-mentioned results unfortunately make the extrapolation from the strand through the short sample and finally to the coil performance not fully predictable at present, at least in the case of the TFMC conductor considered here.

Acknowledgments

EFDA and MIUR partially financially supported the work of RZ and LSR. We thank M Bagnasco for running the M&M code.

References

Ciazynski D, Duchateau J L, Schild T and Fuchs A M 2000 Test results and analysis of two European full-size conductor samples for ITER *IEEE Trans. Appl. Supercond.* **10** 1058–61

Duchateau J L *et al* 2001 Electromagnetic evaluation of the collective behavior of 720 twisted strands for the TF model coil experiment *IEEE Trans. Appl. Supercond.* **11** 2026–9

Duchateau J L *et al* 2004 Exploring the limits of a very large Nb_3Sn conductor: the 80 kA conductor of the ITER toroidal field model coil *Supercond. Sci. Technol.* **17** 241–9

Godeke A *et al* 1998 Characterization of ITER strands in the frame of the third Benchmark tests *Report UT-NET 98-5*

Hamada K *et al* 2002 Hydraulic characteristics of ITER TF insert coil–electromagnetic force effect on hydraulic performance *Cryog. Eng.* **37** 21–8 (in Japanese)

Heller R, Ciazynski D, Duchateau J L, Marchese V, Savoldi Richard L and Zanino R 2003 Evaluation of the current sharing temperature of the ITER toroidal field model coil *IEEE Trans. Appl. Supercond.* **13** 1447–51

ITER Design Description Document 2004 DDD11, Magnets, Section 1, Engineering Description *ITER Project Documentation,* N11DDD178 04-06-04 R0.4

Lee P J, Squitieri A A and Larbalestier D C 2000 Nb_3Sn: macrostructure, microstructure, and property comparisons for bronze and internal Sn process strands *IEEE Trans. Appl. Supercond.* **10** 979–82

Martinez A *et al* 1997 Field and temperature dependencies of critical current on industrial NbSn strands *Cryogenics* **37** 865–75

Mitchell N 2000 Steady state analysis of non-uniform current distributions in cable-in-conduit conductors and comparison with experimental data *Cryogenics* **40** 99–116

Mitchell N 2003 Mechanical and magnetic load effects in Nb_3Sn cable-in-conduit conductors *Cryogenics* **43** 255–70

Nijhuis A *et al* 2004 Performance of an ITER CS1 model coil conductor under transverse cyclic loading up to 40000 cycles *IEEE Trans. Appl. Supercond.* **14** 1489–94

Raff S, Schanz P, Fillunger H and Glaßl B 2001 Structural analysis and verification of the ITER TF model coil test conditions *Fusion Eng. Des.* **58/59** 247–51

Savoldi L and Zanino R 2000 M&M: multi-conductor Mithrandir Code for the simulation of thermal-hydraulic transients in super-conducting magnets *Cryogenics* **40** 179–89

Savoldi L, Zanino R, Marchese V, Martovetsky N, Suesser M, Ulbricht A, Wuechner F and Zahn G 2002 First measurement of the current sharing temperature at 80 kA in the ITER Toroidal Field Model Coil (TFMC) *IEEE Trans. Appl. Supercond.* **12** 635–8

Savoldi Richard L, Mitchell N and Zanino R 2005 From short sample to coil DC superconductor performance: ITER Central Solenoid Model Coil (CSMC) versus Good Joint (GJ) sample *Presented at MT-19 (Genova, Italy, Sept. 2005)*; *IEEE Trans. Appl. Supercond.* submitted

Schild T, Ciazynski D and Court S 2000 Effect of actual cabling pattern on the critical current of a multistage CICC *Adv. Cryog. Eng. B* **46** 1051–8

Summers L T, Guinan M W, Miller J R and Hahn P A 1991 A model for the prediction of Nb3Sn critical current as a function of field, temperature, strain and radiation damage *IEEE Trans. Magn.* **27** 2041–4

Taylor D M J and Hampshire D P 2005 The strain dependence of the critical current density in advanced Nb_3Sn superconducting wires *Supercond. Sci. Technol.* at press

Ulbricht A *et al* 2005 The ITER toroidal field model coil project *Fusion Eng. Des.* **73** 189–327

Zanino R *et al* 2004 T_{CS} tests and performance assessment of the ITER toroidal field model coil (phase II) *IEEE Trans. Appl. Supercond.* **14** 1519–22

Zanino R, Mitchell N and Savoldi Richard L 2003a Analysis and interpretation of the full set (2000–2002) of T_{CS} tests in conductor 1A of the ITER central solenoid model coil *Cryogenics* **43** 179–97

Zanino R and Savoldi Richard L 2003 Performance evaluation of the ITER toroidal field model coil phase I. Part 2: M&M analysis and interpretation *Cryogenics* **43** 91–100

Zanino R, Savoldi Richard L and TFMC Testing Group 2003b Performance evaluation of the ITER toroidal field model coil phase I. Part 1: current sharing temperature measurement *Cryogenics* **43** 79–90